optica

Dispersion dynamics of quantum cascade lasers

David Burghoff,[1,*] Yang Yang,[1] John L. Reno,[2] and Qing Hu[1]

[1]Department of Electrical Engineering and Computer Science, Research Laboratory of Electronics, Massachusetts Institute of Technology, Cambridge, Massachusetts 02139, USA
[2]Center for Integrated Nanotechnology, Sandia National Laboratories, Albuquerque, New Mexico 87123, USA
*Corresponding author: burghoff@mit.edu

Received 29 August 2016; revised 21 October 2016; accepted 24 October 2016 (Doc. ID 274720); published 14 November 2016

A key parameter underlying the efficacy of any nonlinear optical process is group velocity dispersion. In quantum cascade lasers (QCLs), there have been several recent demonstrations of devices exploiting nonlinearities in both the mid-infrared and the terahertz. Though the gain of QCLs has been well studied, the dispersion has been much less investigated, and several questions remain about its dynamics and precise origin. In this work, we use time-domain spectroscopy to investigate the dispersion of broadband terahertz QCLs, and demonstrate that contributions from both the material and the intersubband transitions are relevant. We show that in contrast to the laser gain—which is clamped to a fixed value above lasing threshold—the dispersion changes with bias even above threshold, which is a consequence of shifting intersubband populations. We also examine the role of higher-order dispersion in QCLs and discuss the ramifications of our result for devices utilizing nonlinear effects, such as frequency combs.

OCIS codes: (140.5965) Semiconductor lasers, quantum cascade; (140.5960) Semiconductor lasers.

http://dx.doi.org/10.1364/OPTICA.3.001362

Group velocity dispersion is a fundamental parameter of any optical system. Quantum cascade lasers (QCLs) are a semiconductor source of coherent radiation in the mid-infrared and terahertz (THz) [1], and their high powers and large nonlinearities have led to several interesting devices exploiting nonlinear effects. For example, impressive results have been obtained in generating Thz radiation from mid-infrared structures via difference-frequency generation [2–4], active mode locking has been achieved [5–7], and as of late there has been an explosion in research in using QCLs to generate frequency combs [8–12]. Mid-infrared difference-frequency generation can be used to generate continuous wave THz radiation without the need for cryocoolers, and frequency combs can be used to perform coherent broadband spectroscopy [13–15] or to perform broadband tomography [16]. For frequency combs, it is well known that group velocity dispersion (GVD) plays a critical role in the formation of stable combs: in the time domain, GVD causes temporal walk-off between light of different frequencies, and in the frequency domain, GVD causes cavity modes to be spaced non-uniformly. It is for this reason there has been a flurry of activity in the dispersion engineering of QCL cavities, first in the THz [9] and more recently in the mid-infrared [17]. Many dispersion compensation schemes have now been demonstrated, including double-chirped mirrors [9,18,19] and other geometries [17,20].

Of course, before one can effectively engineer the dispersion of a cavity, one must first understand the various contributions to the GVD. Although gain and dispersion are essentially two sides to the same coin (linear susceptibility), the dispersion is in general much more difficult to measure. Whereas the gain spectrum is made apparent by the lasing and electroluminescence spectra, dispersion characterization requires various types of broadband interferometry. In the mid-infrared, this can be done by high-resolution spontaneous emission measurements [21,22] or broadband transmission measurements [2,23]; in the THz, the weak spontaneous emission necessitates the use of terahertz time-domain spectroscopy (THz-TDS) [24–27]. Though one can of course simulate the intersubband-induced dispersion via density-matrix-based approaches, the results are lacking when compared with experiment for the same reason that intersubband gain is often difficult to predict (e.g., uncertainty in the growth parameters, uncertainty in the simulation parameters). The difficulty of dispersion measurements has hampered the understanding of the various contributors to dispersion in QCLs, particularly those due to the intersubband transitions. As a result, several questions remain unanswered about the dispersion dynamics of QCLs: How does the dispersion of QCLs change above and below lasing threshold? What factors contribute significantly to the dispersion? What is the role of higher-order dispersion, if any?

For this study, we focus on the dispersion dynamics of a broadband THz QCL structure, whose basic properties are shown in Fig. 1. This structure is a homogeneous resonant-phonon structure similar to the one used in Ref. [9], but with several modifications that allow it to achieve continuous bandwidth coverage of 1 THz. The thicker collector barrier reduces the splitting that had previously been observed in similar devices, allowing for gapless continuous coverage. The thicker injector barrier increases the injection selectivity but also reduces the amount of gain available to the main lasing transition. As a result, electrons can pile up in the second injector level (state 1′), and fewer are injected into the upper lasing level (state 5). The net effect of this is that the maximum operating temperature drops (from 176 to 144 K), and

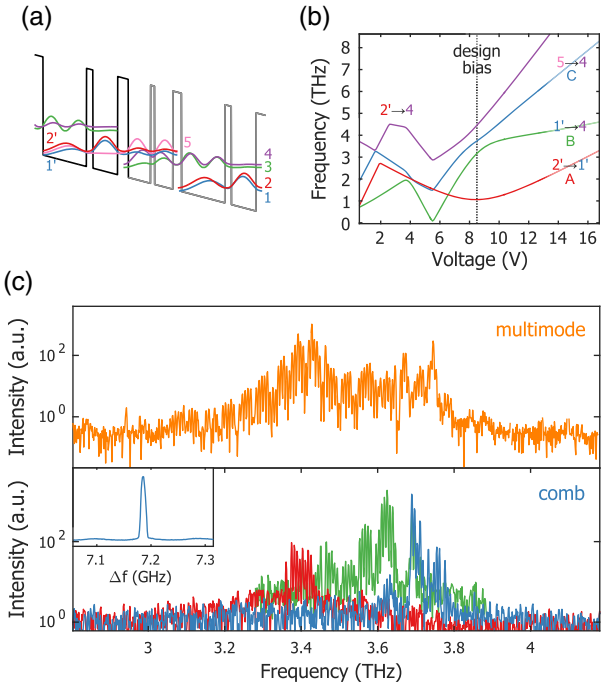

Fig. 1. (a) Wavefunctions and (b) energy differences of the THz QCL under study. Starting from the injector barrier, the layer thicknesses in monolayers are **16**/33.5/**6**/27.5/**13**/65/**9.5**/37 (barriers in bold). (c) Top: broadband low-temperature emission of gain medium, showing a 1 THz span. Bottom: spectrum of 4 mm laser operated in a 700 GHz spanning comb regime, with second-order compensation of 0.88 ps^2. The device is operated at 12 V and 48 K, different spectra indicate different spectral filters, and the inset shows the beatnote.

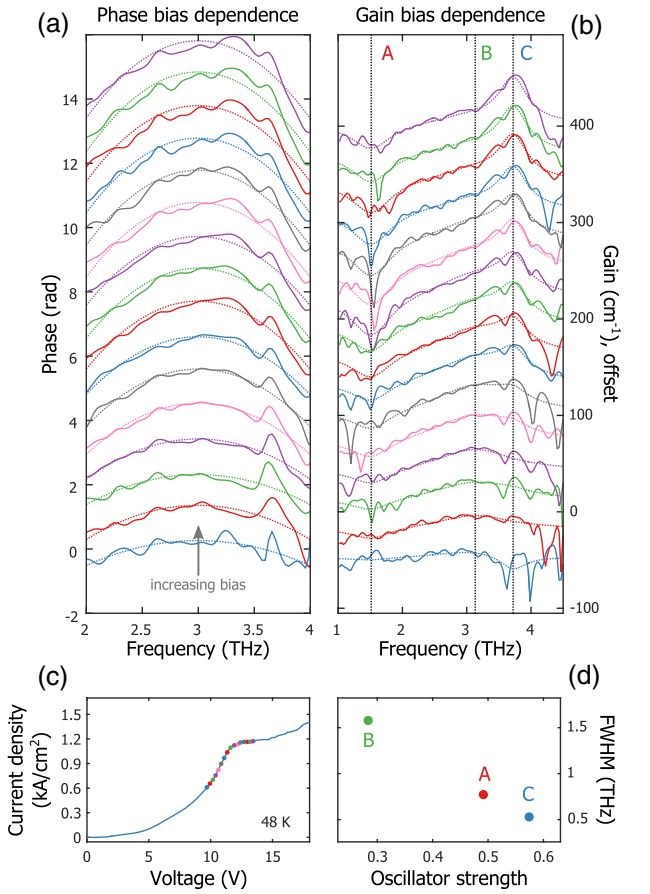

Fig. 2. (a) Bias dependence of the round-trip phase associated with pulse propagation at 48 K. Parabolic fits in dashed lines. (b) Bias dependence of the round-trip gain, offset by 30 cm^{-1}. Dashed lines indicate triple-Lorentzian fit. (c) Current-voltage of the pumped device, with the bias points of (a) and (b) highlighted. (d) Simulated oscillator strengths at design bias versus best fit linewidths.

lasing between states 1′ and 4 is enabled. Qualitatively, this gain medium is similar to continuum-to-bound structures that have been demonstrated in the mid-infrared [28]. The three transitions in this system that are spectroscopically accessible are the intra-injector absorption ($1' \rightarrow 2'$, labeled A) and the two lasing transitions ($1' \rightarrow 4$, labeled B, and $5 \rightarrow 4$, labeled C).

The maximum operating bandwidth of this gain medium, shown in Fig. 1(c), is approximately 1 THz, with the broadest coverage being achieved at low biases, near threshold. As we will show, the broadest emission occurs at low biases, because it is here that states 1′ and 5 can be simultaneously populated. (At high biases, only state 5 is heavily populated, and the usual two-level resonant-phonon lasing occurs.) By compensating for an optimal second-order dispersion of 0.11 ps^2/mm using a double-chirped mirror, we are able to achieve a comb spanning 700 GHz [shown in Fig. 1(c)]. A grating and slit were used to verify comb bandwidth [29].

To measure the dispersion of the structure, we use THz-TDS in the self-referenced geometry; for additional details and density matrix simulations refer to Supplement 1. Figure 2 shows the round-trip phase and gain associated with pulse propagation in a 400 μm long waveguide whose current–voltage relation is shown in Fig. 2(c). Phase and gain are measured both below and above threshold. Figure 2(a) shows the phase with the average group delay removed, alongside a parabolic fit over the 2–4 THz range. Since nonlinear phase is associated with dispersion, it is clear that the dispersion is larger at higher biases. In addition, the quality of the parabolic fit degrades noticeably at high biases, indicating that higher-order dispersion becomes more relevant. To investigate the source of this bias dependence, we fit the *gain* data as a function of bias to determine the intersubband absorptions associated with each of the three observed transitions (A, B, and C). To prevent overfitting, we allow only the transition amplitudes to vary with bias (i.e., not the linewidths or frequencies). Transitions A, B, and C are found to have best-fit frequencies of 1.5, 3.1, and 3.7 THz with full width at half-maximums (FWHMs) of 0.77, 1.58, and 0.53 THz, respectively. By comparing the best-fit linewidths to the simulated oscillator strength of each transition at design bias, indicated in Fig. 2(d), we find that the more diagonal transitions yield broader linewidths, as expected.

Armed with the knowledge of the relative intersubband transition strengths, we can now use the Kramers–Kronig relation to investigate their independent contributions to dispersion. Figure 3 shows the round-trip gain over a 1 THz interval as a function of bias, encompassing both the laser frequency (3–4 THz) and the intra-injector frequency (1–2 THz). As expected, the gain clamps to a value slightly below 0 cm^{-1} above threshold, and the intra-injector absorption reaches its maximum slightly above the onset of lasing. In contrast, the second-order GVD, shown in Fig. 3(c), shows no such clamping. (For now, we

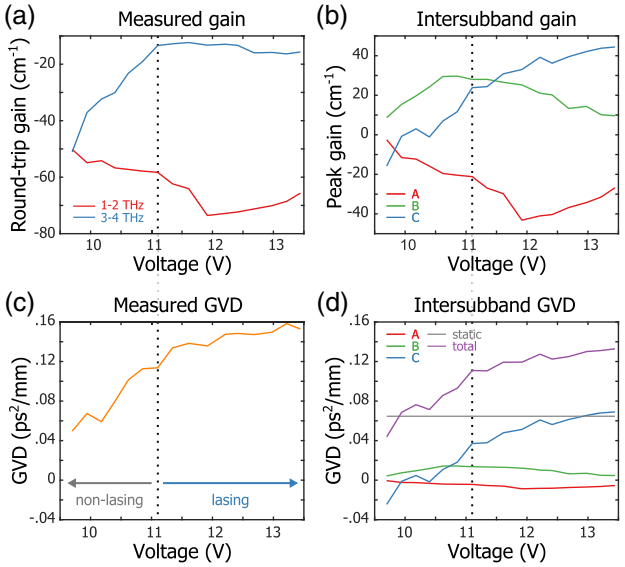

Fig. 3. (a) Overall intra-injector absorption and laser gain as a function of bias, averaged over a 1 THz interval. Vertical dashed line indicates laser threshold, above which gain clamps. (b) Peak intersubband gain of the three transitions, extracted from the TDS data. (c) Second-order GVD computed over the 2–4 THz interval. Gain is clamped, but dispersion increases above threshold. (d) Contributions of each transition to the second-order GVD, along with the static contribution.

consider only the second-order GVD over the 2–4 THz interval.) The dispersion sharply increases below laser threshold, and continues to rise above threshold, albeit at a more moderate pace. In a simpler laser one might think that the intersubband-induced dispersion would be clamped along with the laser gain since the population inversion is clamped, and this is indeed what has been found in interband semiconductor lasers [30]. Note also that the lack of clamping cannot be explained by a simple frequency shift, as the lasing frequency is always contained within the interval of interest. By plotting the peak intersubband gain associated with each transition [Fig. 3(b)], we can conclusively identify the cause. Even though the total gain is clamped by the action of lasing, the contribution due to transition B reaches its peak around laser threshold, whereas the contribution from transition C reaches its peak far higher. Their sum is constant, but because B has a much broader linewidth than C, it contributes much less dispersion. This can be verified by computing the second-order dispersion associated with the three Lorentzian transitions [Fig. 3(d)], which additionally shows the static (non-intersubband) contribution of dispersion computed from standard theoretical models [31]. Several features are noteworthy. First, even though the loss due to transition A varies quite a bit above threshold, it contributes very little GVD over the frequency range of interest, since it is out-of-band. Likewise, transition B contributes little GVD, on account of its broad linewidth. It is transition C that contributes almost all of the dynamical dispersion, due to its narrow linewidth and sharp increase even above threshold. The three transitions and static contributions are summed to produce a total that is also plotted in Fig. 3(d), and agrees well with the measured GVD in Fig. 3(c). Essentially, what this shows is that the gain measurement fully accounts for all of the observed GVD (in accordance with

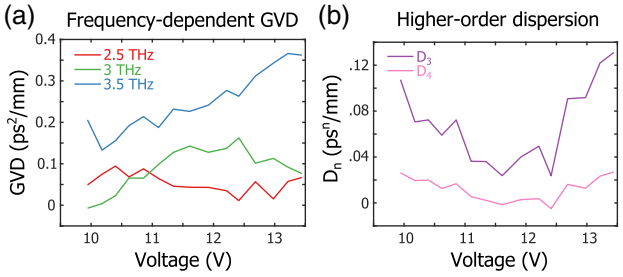

Fig. 4. (a) Frequency-dependent GVD, obtained using a fourth-order fitting over the 2–4 THz interval. (b) Corresponding higher-order dispersion coefficients, specified at 3.5 THz.

Kramers–Kronig), and that the only relevant out-of-band absorption features contributing to dispersion are the standard material contributions. Of course, it is worth pointing out that the static contribution to GVD is not small, accounting for approximately half of the total dispersion even at high biases.

Next, we turn to the issue of higher-order dispersion. As previously mentioned, at high biases, higher-order dispersion becomes more relevant, creating a non-parabolic phase profile, and may need to be compensated for with appropriate dispersion engineering. To avoid overfitting to various TDS artifacts, we consider only dispersion up to fourth order. First, we plot in Fig. 4(a) the second-order GVD (D_2, where $D_n \equiv \frac{1}{2L}\frac{\partial^n \phi}{\partial \omega^n}$) as a function of frequency. At 2.5 THz, far from the peak frequencies of any intersubband transition, the GVD remains small and is essentially fully accounted for by the static GVD. At 3 THz, near the peak of transition B, the dispersion changes non-monotonically, roughly in accordance with transition B's strength. At 3.5 THz, near the peak of transition C, the dispersion changes quite drastically, reaching a peak value of 0.35 ps^2/mm. Once again, this is concordant with the observed strength of transition C. In Fig. 4(b), we plot the higher-order dispersion coefficients at 3.5 THz. It is interesting to note that both D_3 and D_4 change non-monotonically, peaking at low biases and again at high biases (even as D_2 continues to rise). The lowest high-order dispersion occurs at a bias just above threshold where transitions B and C are well balanced, and starts to rise once B begins to weaken.

These results have several implications on the development of QCL-based frequency combs. Clearly, a strong bias dependence of the laser dispersion above threshold is problematic from the standpoint of dispersion engineering, since the dispersion can be compensated effectively at only a single bias point. Particularly in THz QCLs, it has been noted that even with carefully implemented dispersion compensation, the laser can operate in several different comb regimes whose time-domain dynamics are completely different [32]. To our knowledge, no measurement of the dispersion in mid-infrared QCLs has been reported above threshold [17,33], but, even so, the issue may not be as severe since mid-infrared gain lineshapes are typically less bias dependent. One strategy that may be able to remedy these effects is the incorporation of multi-section cavities, which could be used to balance this bias dependence. We have also shown that the higher-order contribution to dispersion is relevant, and since the broadest combs were achieved at moderate biases, it is likely the case that higher-order dispersion still limits the bandwidth. Even though this gain medium is THz-spanning, the maximum comb bandwidth is only 70% of its gain bandwidth, as we have

only compensated D_2. Similarly, in dispersion-compensated mid-infrared gain media [17], the comb bandwidth was 77% of the gain bandwidth, and in uncompensated broadband THz heterogeneous gain media [11,34], the comb bandwidth was 36% of the gain bandwidth. Forunately, the remedy here is straightforward: higher-order dispersion compensation [35] has been used successfully in microresonators to achieve larger bandwidths, and it is likely that such a strategy will also be successful in QCLs.

In conclusion, we have used THz-TDS to probe the dispersion dynamics of THz QCLs. We have shown that both the static and intersubband contributions play critical roles in determining the dispersion of the QCL cavity, and have identified the role of the relevant intersubband transitions. We showed that even when the laser gain is clamped, the intersubband contribution of the GVD has no such constraint, a consequence of the changing lineshape of the gain peak. We showed that higher-order dispersion may play a key role in determining the bandwidth available for comb formation, and discussed several strategies for mitigating these effects in combs.

Funding. Defense Advanced Research Projects Agency (DARPA) (W31P4Q-16-1-0001); National Science Foundation (NSF); Sandia National Laboratories; U.S. Department of Energy (DOE) (DE-AC04-94AL85000).

Acknowledgment. The authors thank Sushil Kumar of Lehigh University for designing the gain medium.

See Supplement 1 for supporting content.

REFERENCES

1. J. Faist, F. Capasso, D. L. Sivco, C. Sirtori, A. L. Hutchinson, and A. Y. Cho, Science **264**, 553 (1994).
2. Y. Jiang, K. Vijayraghavan, S. Jung, A. Jiang, J. H. Kim, F. Demmerle, G. Boehm, M. C. Amann, and M. A. Belkin, Sci. Rep. **6**, 21169 (2016).
3. Q. Lu, D. Wu, S. Sengupta, and S. Slivken, Sci. Rep. **6**, 1 (2016).
4. B. A. Burnett and B. S. Williams, Phys. Rev. Appl. **5**, 034013 (2016).
5. D. G. Revin, M. Hemingway, Y. Wang, J. W. Cockburn, and A. Belyanin, Nat. Commun. **7**, 11440 (2016).
6. S. Barbieri, M. Ravaro, P. Gellie, G. Santarelli, C. Manquest, C. Sirtori, S. P. Khanna, E. H. Linfield, and A. G. Davies, Nat. Photonics **5**, 306 (2011).
7. F. Castellano, L. Li, E. H. Linfield, A. G. Davies, and M. S. Vitiello, Sci. Rep. **6**, 23053 (2016).
8. A. Hugi, G. Villares, S. Blaser, H. C. Liu, and J. Faist, Nature **492**, 229 (2012).
9. D. Burghoff, T.-Y. Kao, N. Han, C. W. I. Chan, X. Cai, Y. Yang, D. J. Hayton, J.-R. Gao, J. L. Reno, and Q. Hu, Nat. Photonics **8**, 462 (2014).
10. M. Wienold, B. Röben, L. Schrottke, and H. T. Grahn, Opt. Express **22**, 30410 (2014).
11. M. Rösch, G. Scalari, M. Beck, and J. Faist, Nat. Photonics **9**, 42 (2014).
12. Q. Y. Lu, M. Razeghi, S. Slivken, N. Bandyopadhyay, Y. Bai, W. J. Zhou, M. Chen, D. Heydari, A. Haddadi, R. McClintock, M. Amanti, and C. Sirtori, Appl. Phys. Lett. **106**, 051105 (2015).
13. Y. Wang, M. G. Soskind, W. Wang, and G. Wysocki, Appl. Phys. Lett. **104**, 031114 (2014).
14. G. Villares, A. Hugi, S. Blaser, and J. Faist, Nat. Commun. **5**, 5192 (2014).
15. Y. Yang, D. Burghoff, D. J. Hayton, J.-R. Gao, J. L. Reno, and Q. Hu, Optica **3**, 499 (2016).
16. A. W. M. Lee, T.-Y. Kao, D. Burghoff, Q. Hu, and J. L. Reno, Opt. Lett. **37**, 217 (2012).
17. G. Villares, S. Riedi, J. Wolf, D. Kazakov, M. J. Süess, P. Jouy, M. Beck, and J. Faist, Optica **3**, 252 (2016).
18. J. Faist, G. Villares, G. Scalari, M. Rösch, C. Bonzon, A. Hugi, and M. Beck, Nanophotonics **5**, 272 (2016).
19. C. Xu and D. Ban, Opt. Express **24**, 13500 (2016).
20. T. Fobbe, S. Markmann, F. Fobbe, N. Hekmat, H. Nong, S. Pal, P. Balzerwoski, J. Savolainen, M. Havenith, A. D. Wieck, and N. Jukam, Opt. Express **24**, 22319 (2016).
21. B. W. Hakki and T. L. Paoli, J. Appl. Phys. **46**, 1299 (1975).
22. D. Hofstetter and J. Faist, IEEE Photon. Technol. Lett. **11**, 1372 (1999).
23. D. G. Revin, L. R. Wilson, J. W. Cockburn, A. B. Krysa, J. S. Roberts, and R. J. Airey, Appl. Phys. Lett. **88**, 131105 (2006).
24. J. Kröll, J. Darmo, S. S. Dhillon, X. Marcadet, M. Calligaro, C. Sirtori, and K. Unterrainer, Nature **449**, 698 (2007).
25. N. Jukam, S. Dhillon, Z.-Y. Zhao, G. Duerr, J. Armijo, N. Sirmons, S. Hameau, S. Barbieri, P. Filloux, C. Sirtori, X. Marcadet, and J. Tignon, IEEE J. Sel. Top. Quantum Electron. **14**, 436 (2008).
26. D. Burghoff, T. Y. Kao, D. Ban, A. W. M. Lee, Q. Hu, and J. Reno, Appl. Phys. Lett. **98**, 061112 (2011).
27. D. Burghoff, C. W. I. Chan, Q. Hu, and J. L. Reno, Appl. Phys. Lett. **100**, 261111 (2012).
28. Y. Yao, W. O. Charles, T. Tsai, J. Chen, G. Wysocki, and C. F. Gmachl, Appl. Phys. Lett. **96**, 211106 (2010).
29. M. Wienold, B. Röben, L. Schrottke, and H. T. Grahn, Proc. SPIE **9767**, 97671A (2016).
30. R. Gordon, A. P. Heberle, and J. R. A. Cleaver, J. Opt. Soc. Am. B **21**, 29 (2004).
31. J. S. Blakemore, J. Appl. Phys. **53**, R123 (1982).
32. D. Burghoff, Y. Yang, D. J. Hayton, J.-R. Gao, J. L. Reno, and Q. Hu, Opt. Express **23**, 1190 (2015).
33. W. Parz, T. Müller, J. Darmo, M. Austerer, G. Strasser, L. Wilson, J. Cockburn, A. Krysa, J. Roberts, and K. Unterrainer, Opt. Lett. **34**, 208 (2009).
34. D. Bachmann, M. Rösch, C. Deutsch, M. Krall, G. Scalari, M. Beck, J. Faist, K. Unterrainer, and J. Darmo, Appl. Phys. Lett. **105**, 181118 (2014).
35. Y. Okawachi, M. R. E. Lamont, K. Luke, D. O. Carvalho, M. Yu, M. Lipson, and A. L. Gaeta, Opt. Lett. **39**, 3535 (2014).